2013

The global NPP dependence on ENSO: La Niña and the extraordinary year of 2011

A. Bastos
Universidade de Lisboa

Steven W. Running
University of Montana - Missoula

Célia M. Gouveia
Universidade de Lisboa, Lisboa, Portugal

Ricardo M. Trigo
Universidade de Lisboa, Lisboa, Portugal

Recommended Citation
Bastos, A., S. W. Running, C. Gouveia, and R. M. Trigo (2013), The global NPP dependence on ENSO: La Niña and the extraordinary year of 2011, J. Geophys. Res. Biogeosci., 118, 1247-1255, doi:10.1002/jgrg.20100

JOURNAL OF GEOPHYSICAL RESEARCH: BIOGEOSCIENCES, VOL. 118, 1–9, doi:10.1002/jgrg.20100, 2013

The global NPP dependence on ENSO: La Niña and the extraordinary year of 2011

A. Bastos,[1,2] Steven W. Running,[2] Célia Gouveia,[1,3] and Ricardo M. Trigo[1,3]

Received 30 May 2013; revised 23 July 2013; accepted 25 July 2013.

[1] Global ecosystems remove about 25% of anthropogenic CO_2 emissions; however, the response of the land sink to climate variability and change is not yet fully understood. In 2011, the highest global value of net primary production (NPP) since 2000 was registered on the Moderate Resolution Imaging Spectroradiometer record, together with the highest value on the Carbon Dioxide Information Analysis Center record of carbon land sink strength since 1959. Here we show that El Niño/Southern Oscillation (ENSO) is responsible for much of the variability observed in the land sink and that the high NPP anomaly observed in 2011 was largely influenced by the strongest La Niña since the 1970s that lasted from late 2010 to early 2012. ENSO explains more than 40% of global NPP variability, mainly driven by the response of Southern Hemisphere ecosystems, particularly in tropical and subtropical regions. Water availability, controlled by temperature and precipitation anomalies, appears to be the main factor driving the regional response of NPP to ENSO.

Citation: Bastos, A., S. W. Running, C. Gouveia, and R. M. Trigo (2013), The global NPP dependence on ENSO: La Niña and the extraordinary year of 2011, *J. Geophys. Res. Biogeosci.*, *118*, doi:10.1002/jgrg.20100.

1. Introduction

[2] Anthropogenic CO_2 emissions from fossil fuel burning and land-use change have been increasing since the 1960s. Each year, about half of anthropogenic emissions remain in the atmosphere, being the remaining half absorbed by land and oceans sinks [*Le Quéré et al.*, 2009]. In the last decades, these sinks presented an increasing strength but also considerable interannual variability. As the ocean sink reveals a relatively smooth behavior, with a slight increasing trend and low year-to-year variability, most of the variability observed in the airborne fraction is due to the very high interannual variability of the land sink [*Le Quéré et al.*, 2009; *Raupach*, 2011; *Ballantyne et al.*, 2012].

[3] There is, however, a great debate about whether the increase in CO_2 uptake has been maintained since the beginning of this century [*Zhao and Running*, 2010; *Samanta et al.*, 2011; *Ahlström et al.*, 2012]. Several studies have stressed the complex response of ecosystems to the wide range of climate variables affecting carbon uptake by ecosystems, such as temperature, precipitation and solar radiation [*Nemani et al.*, 2003; *Cox et al.*, 2004; *Huete et al.*, 2006; *Beer et al.*, 2010], the length of the growing season [*Piao et al.*, 2008], and extreme events [*Ciais et al.*, 2005; *Samanta et al.*, 2010]. Uncertainties about the magnitude and future behavior of the terrestrial carbon sink are still high, mainly as a consequence of high interannual variability and the response of regional ecosystems to changes in climate forcings [*Raupach*, 2011; *Ballantyne et al.*, 2012].

[4] The El Niño/Southern Oscillation (ENSO), one of the main large-scale coupled modes of circulation, affects climate patterns and interannual variability worldwide. Previous studies have suggested that ENSO may have an influence on net primary production (NPP) [*Behrenfeld et al.*, 2001; *Nemani et al.*, 2003], the magnitude of the land sink [*Le Quéré et al.*, 2009; *Raupach*, 2011], and atmospheric CO_2 growth rate [*Heimann and Reichstein*, 2008; *Friedlingstein and Prentice*, 2010; *Ballantyne et al.*, 2012], with El Niño apparently associated to years with low global NPP and higher CO_2 accumulation in the atmosphere. However, the nature and strength of this relationship, as well as the main driving physical mechanisms, have not, as yet, been addressed in detail.

[5] This works aims to evaluate the relationship between the interannual variability of the land sink and ENSO and, in particular, to identify the regions driving this relationship as well as the most relevant climate factors forcing the response of ecosystems to ENSO. Finally, we intend to understand whether the increased carbon uptake by ecosystems observed in 2011 was a response to the strong contemporary La Niña.

[6] We first analyze the long (1959–2011) Carbon Dioxide Information Analysis Center (CDIAC) global land CO_2 uptake [*Le Quéré et al.*, 2012] data set. However, this data set provides only global values and, thus, the shorter (2000–2011) data set of Moderate Resolution Imaging

[1]Instituto Dom Luiz, Universidade de Lisboa, Lisboa, Portugal.
[2]Numerical Terradynamic Simulation Group, University of Montana, Missoula, Montana, USA.
[3]Universidade Lusófona, Lisboa, Portugal.

Corresponding author: A. Bastos, Instituto Dom Luiz, Universidade de Lisboa, Campo Grande, Ed. C8, Piso 3, Sala 8.3.15, 1749-016 Lisboa, Portugal. (afbastos@fc.ul.pt)

2169-8953/13/10.1002/jgrg.20100

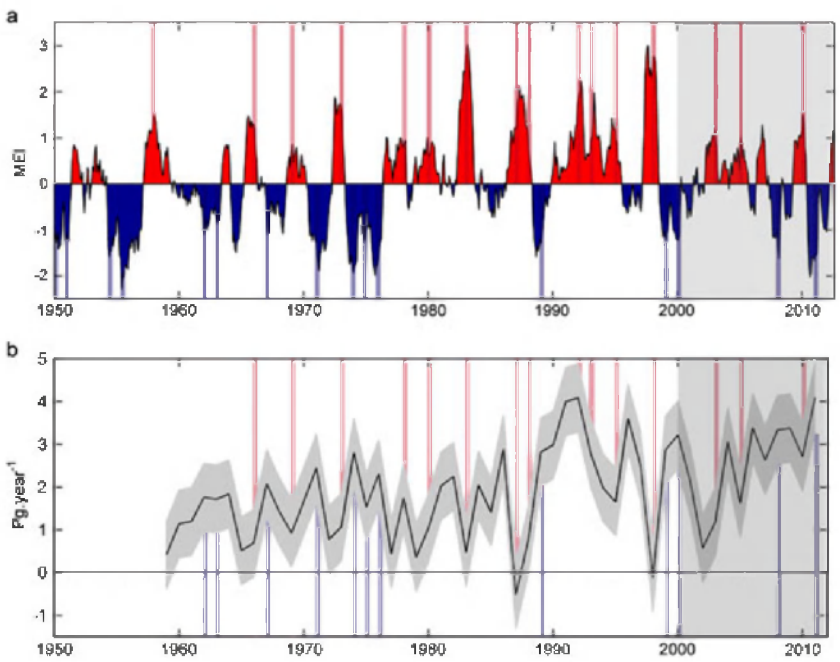

Figure 1. ENSO and land carbon uptake variability. (a) Bimonthly Multivariate ENSO Index from Dec/Jan 1950 to Jul/Aug 2012 provided by NOAA-CPC, positive values correspond to El Niño and negative values to La Niña. (b) Land CO_2 uptake (S_{land}) from CDIAC (black) and associated uncertainty (grey-shaded interval). Red (blue) shades indicate the strongest warm (cold) winter ENSO composites, calculated as the upper (lower) quartile of the record. The period analyzed in detail in the present work is highlighted in light grey.

Spectroradiometer (MODIS)-NPP global fields [*Zhao and Running*, 2010] was simultaneously used to perform spatial analysis. Although the CDIAC data set corresponds to the net CO_2 flux of global ecosystems (Net Ecosystem Exchange, i.e., NPP minus ecosystem respiration), the interannual variability of NPP and ecosystem respiration was shown to be closely related in previous studies [*Chapin et al.*, 2006]. Therefore, their complementary use in this study increases the robustness of the results and allows a more detailed analysis of spatial variability patterns.

[7] We find a strong anticorrelation between ENSO and NPP, which is mostly driven by ecosystems at tropical and subtropical latitudes. We also find water availability, through combined temperature and precipitation anomalies, to be the key factor governing the response of NPP to ENSO variability.

[8] The remarkable La Niña event had, thus, a strong influence on the enhanced carbon uptake by ecosystems observed in 2011. Moreover, results highlight the importance of large-scale climate variability modes on the land sink dynamics.

2. Data and Methods

[9] A long data set of land CO_2 uptake developed by the Global Carbon Project was extracted from the Carbon Dioxide Information Analysis Center (CDIAC). This data set provides information about the magnitude of the land sink (S_{land}) and respective uncertainties from 1959 to 2011, which are computed indirectly from the atmospheric CO_2 accumulation and uptake by ocean to the global CO_2 emissions (fossil fuels and land-use change) as described in *Le Quéré et al.* [2012]. S_{land} corresponds to the net CO_2 flux of global ecosystems (i.e., NPP minus ecosystem respiration). The interannual variability of S_{land} is related to NPP variability [*Chapin et al.*, 2006], and S_{land} is used as a complementary and independent data set for assessing NPP variability.

[10] The spatial analysis in this work relies on the improved MOD17A3 annual global NPP data set which is derived from the MODIS-NPP algorithm [*Running et al.*, 2004] and driven by daily meteorological data from the National Centers for Environmental Prediction (NCEP)/Department of Energy (DOE) II Reanalyzes as described in *Zhao and Running* [2010]. This data set has been regularly updated and now encompasses a 12 year period spanning from 2000 to 2011 and covering the regions between 80°N and 60°S at 1 km spatial resolution. Annual NPP anomaly (hereafter NPP_{anom}) fields were computed as the annual departure from the long-term average in the study period. Global and hemispheric values of annual NPP_{anom} were finally computed as the integrated NPP_{anom} restricted to vegetated area.

[11] For climate assessment, monthly means of average air temperature fields at 2 m, incoming short wave radiation flux at the surface, and soil wetness (volumetric) in the top (2 cm depth) and root (1 m depth) layers, defined as the ratio between volumetric water to the porosity, were extracted from the National Aeronautics and Space Administration (NASA)/(GMAO MERRA) Global Modeling and Assimilation Office and Modern-Era Retrospective Analysis for Research and Applications Reanalyzes [*Rienecker et al.*,

2011] which provide global fields from 1979 to present at 0.5° resolution. Annual average fields were computed for the whole period and are henceforth referred as T_{avg} (temperature), R_{avg} (incoming short wave radiation flux), GW_{top}, and GW_{root} (soil wetness at the top 2 cm and top meter layers, respectively).

[12] This work relies essentially on NASA/GMAO MERRA temperature records since it is an independent database from NCEP/DOE II Reanalyzes [*Kanamitsu et al.*, 2002], which were only used for comparison purposes.

[13] Monthly precipitation data were extracted from the Global Precipitation Climatology Centre monitoring product which is based on near real-time rain gauge observations and provides monthly mean global precipitation fields between 1986 and present at 1° spatial resolution [*Rudolf and Schneider*, 2005]. Annual accumulated precipitation fields (P_{total}) were computed as the sum of monthly values over the period 1986–2011.

[14] Many indices related with the El Niño/Southern Oscillation (ENSO) phenomena have been proposed in the literature. Here we used the Multivariate ENSO Index (MEI) provided by National Oceanic and Atmospheric Administration's Climate Prediction Center (NOAA-CPC). MEI bimonthly values are provided since 1950 to 2012. A winter ENSO composite was calculated as the mean MEI values observed between Dec/Jan and Mar/Apr for each year and is henceforth referred to as MEI_w.

[15] The complete record (1950–2012) was used to calculate the threshold for warm (cold) events, defined as the upper (lower) quartile of the record. Positive and negative ENSO phases, corresponding to El Niño or La Niña (respectively, $ENSO^+$ and $ENSO^-$) were defined as those years with MEI_w above the warm threshold for $ENSO^+$ and below the cold threshold for $ENSO^-$ (Figure 1a). Based on these thresholds, the events found for the 2000–2011 record are 2002/2003, 2004/2005, and 2009/2010 ($ENSO^+$) and 1999/2000, 2007/2008, and 2010/2011 ($ENSO^-$) and ENSO composites (positive or negative) were then computed for all climate variables.

[16] A preliminary evaluation of the relationship between S_{land} and global NPP was made by computing the correlation between detrended S_{land} and NPP_{anom} for the period 2000–2011, common to both records.

[17] In order to evaluate the relationship between ENSO and global carbon uptake, we computed correlation coefficients between detrended S_{land} and MEI_w for both the long (1959–2011) and shorter (2000–2011) periods. Since the longer time series (S_{land}) does not provide information about spatial variability, the MODIS NPP data set was used for the spatial analysis.

[18] The correlation between global and hemispheric yearly NPP_{anom} and MEI_w was computed to assess the contribution of each hemisphere to the overall relationship. The same procedure was then applied on a pixel by pixel basis to assess the geographic distribution of correlations between the two variables. Regions with high correlations (statistically significant at the 10% level) were selected and the overall correlation between regional NPP_{anom} and ENSO was evaluated.

[19] The impact of ENSO on NPP was assessed by computing the difference between NPP_{anom} composites corresponding to $ENSO^+$ and $ENSO^-$ phases over the period between 2000 and 2011. To understand which climate variables were driving NPP response to ENSO, the differences between composites of T_{avg}, R_{avg}, P_{total}, GWtop and GWroot for $ENSO^+$ and $ENSO^-$ phases between 2000 and 2011 were accordingly analyzed. These differences were also computed for the long record for each variable to assure that results were not influenced by the occurrence of a few exceptional events. In general, there are no appreciable differences between the two procedures, in particular over the regions considered in this work. Finally, results were summarized in maps corresponding to the combination of the positive or negative response of each variable.

3. Results and Discussion

3.1. The Exceptional Year of 2011

[20] Generally, El Niño phases are associated to drier than average conditions in northeastern South America, South Africa, Australia, and the Pacific Basin while wetter conditions are observed on the northwest and southeast coasts of South America and on the Gulf Coast [*Mason and Goddard*, 2001; *Marengo*, 2004; *McPhaden et al.*, 2006]. Likewise, El Niño impinges warmer temperatures on northern, western, and southeastern South America, South Africa, Australia, and on most of the Indian basin, while cooler temperatures prevail over southeastern USA [*Diaz et al.*, 2001]. Accordingly, it has been shown that the occurrence of drought events in these areas is controlled to a large extent by ENSO signal, with drier than usual conditions in tropical and subtropical thriving for long temporal scales (up to 12 months) during El Niño phase [*Vicente-Serrano et al.*, 2011]. During La Niña conditions, the climate patterns are approximately reversed.

[21] In late 2010, ENSO evolved from a moderate El Niño phase to one of the strongest La Niña episodes in the instrumental record, lasting for 2011 and early 2012 (Figure 1a). The strong La Niña episode was associated with a generalized reduction in global surface temperatures (however, still above the 1981–2010 average) and to generally wet conditions [*Blunden and Arndt*, 2012]. This intense episode of La Niña has been shown to lead to a temporary decrease of the mean sea level [*Boening et al.*, 2012] associated with a significant increase in water retention on land, especially in Australia, South Africa, and northern South America [*Boening et al.*, 2012; *Evans and Boyer-Souchet*, 2012].

[22] In the CDIAC land sink magnitude record (S_{land}), 2011 corresponds to the maximal land sink strength since 1959, being only equaled by the value observed in 1992, totaling 4.09 Pg (Figure 1b). The 1992 land sink enhancement has been attributed to the cooler than average conditions following the Mt. Pinatubo eruption in 1991 [*Jones and Cox*, 2001; *Sarmiento et al.*, 2010].

[23] The year 2011 also registered the highest value on the MODIS-NPP record, with global NPP amounting to over 55 Pg (NPP_{anom}=1.54 Pg), following a decade of apparent decrease [*Zhao and Running*, 2010]. The global NPP_{anom} field for 2011 (Figure 2) reveals widespread positive anomalies, corresponding to 51% of vegetated area (against 32% with negative anomalies), and particularly high anomalies (above 0.12 kg m^{-2} $year^{-1}$) throughout most of the Southern Hemisphere (SH), including most of north-

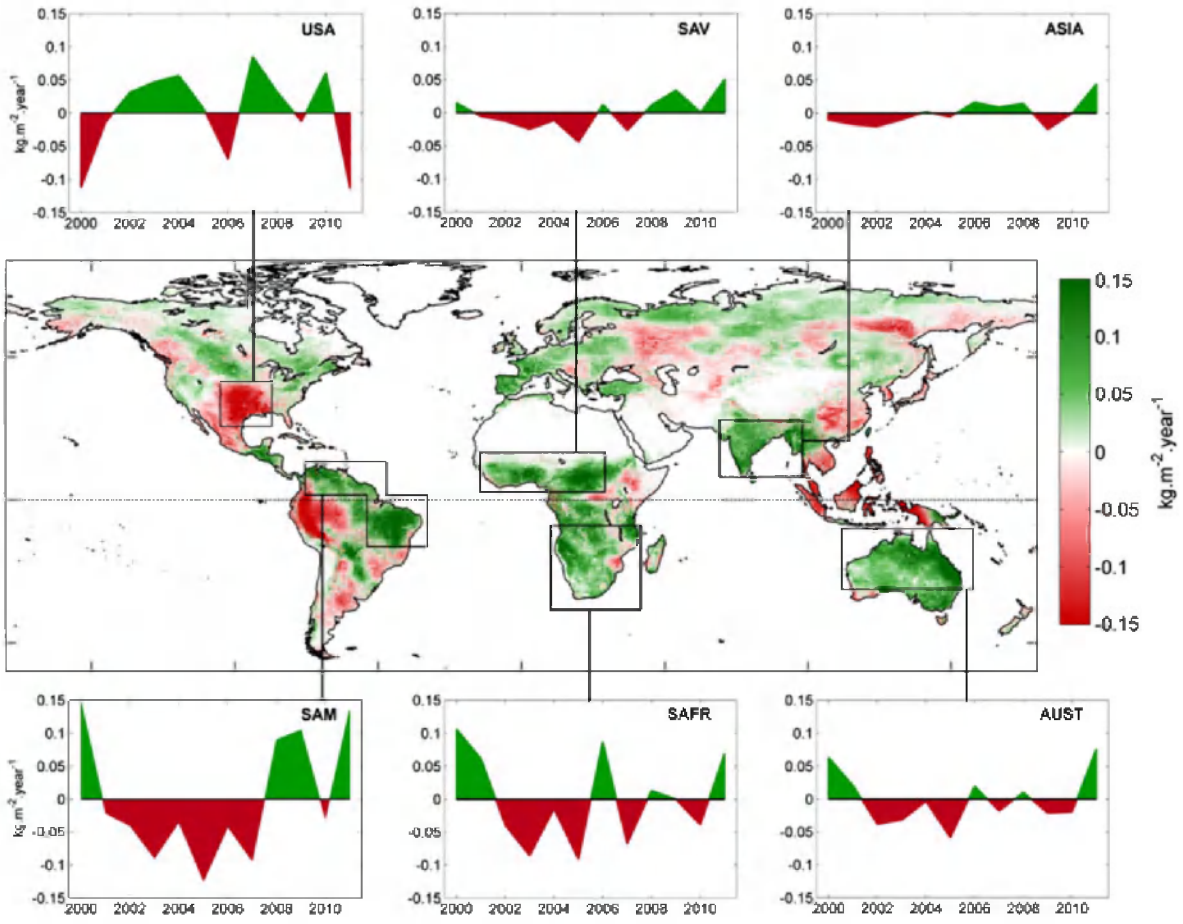

Figure 2. Global NPP anomalies in 2011 and NPP variability in selected regions. Global NPP_{anom} field in 2011 in kg m^{-2} $year^{-1}$ and the evolution of NPP_{anom} over the period 2000–2011 computed in regions with very high absolute anomalies during 2011.

eastern South America (hereafter SAM), southern Africa (SAFR), and Australia (AUST), as indicated by the regional boxes in Figure 2. The main exception in SH corresponds to the northwestern South America and the Asian islands. In the Northern Hemisphere (NH), besides the relatively high values over India and the Bay of Bengal (ASIA), as well as in northern African savannas (SAV), it is also worth pointing the low but widespread positive anomalies in Europe. However, on a hemispheric scale, these anomalies were partially offset by very low negative anomalies on southeastern USA (USA), associated with the outstanding heat wave and drought that struck this region [*Blunden and Arndt*, 2012].

[24] The year 2011 corresponds, thus, to a year of exceptionally strong terrestrial carbon uptake. To assess the influence of the contemporary La Niña episode, the relationship between ENSO and NPP needs to be more deeply understood.

3.2. Linking the Interannual Variability of Carbon Uptake and NPP With ENSO

[25] Despite presenting an apparent positive trend over the 53 year period, S_{land} is characterized by very high interannual variability (Figure 1b). The comparison of the long time series of ENSO (Figure 1a) and S_{land} suggests a negative relationship between ENSO and the magnitude of the land sink, which has been already proposed in several works [*Le Quéré et al.*, 2009; *Raupach*, 2011] but not fully quantified.

[26] A significant anticorrelation between S_{land} and MEI_w over the period 1959–2011 was found ($\rho = -0.53, p \ll 0.01$), with ENSO explaining about 29% of the total variance. However, when restricting the analysis for 2000–2011 (the period used for spatial analysis), anticorrelation was stronger ($\rho = -0.68$, $p = 0.02$), with ENSO dynamics explaining about 46% of S_{land} variability. The lower correlation found for the longer period may be due to the disruption caused by the impact of the two volcanic eruptions, El Chichón in 1982 and Mt. Pinatubo in 1991 [*Jones and Cox*, 2001; *Sarmiento et al.*, 2010]. When removing the years corresponding to each eruption (1982 and 1991) and the subsequent year (1983 and 1992), correlation is much stronger ($\rho = -0.69$, $p \ll 0.01$), stressing the strong opposite effects of volcanic eruptions in the land sink dynamics.

[27] The 2000–2011 NPP record on the most productive regions in 2011 (Figure 2) reveals highly variable dynamics with, however, great differences between the various regions. We must bear in mind that the use of a short time series presents some caveats and that results obtained for some regions (e.g., SAM and AUST) may be biased as a

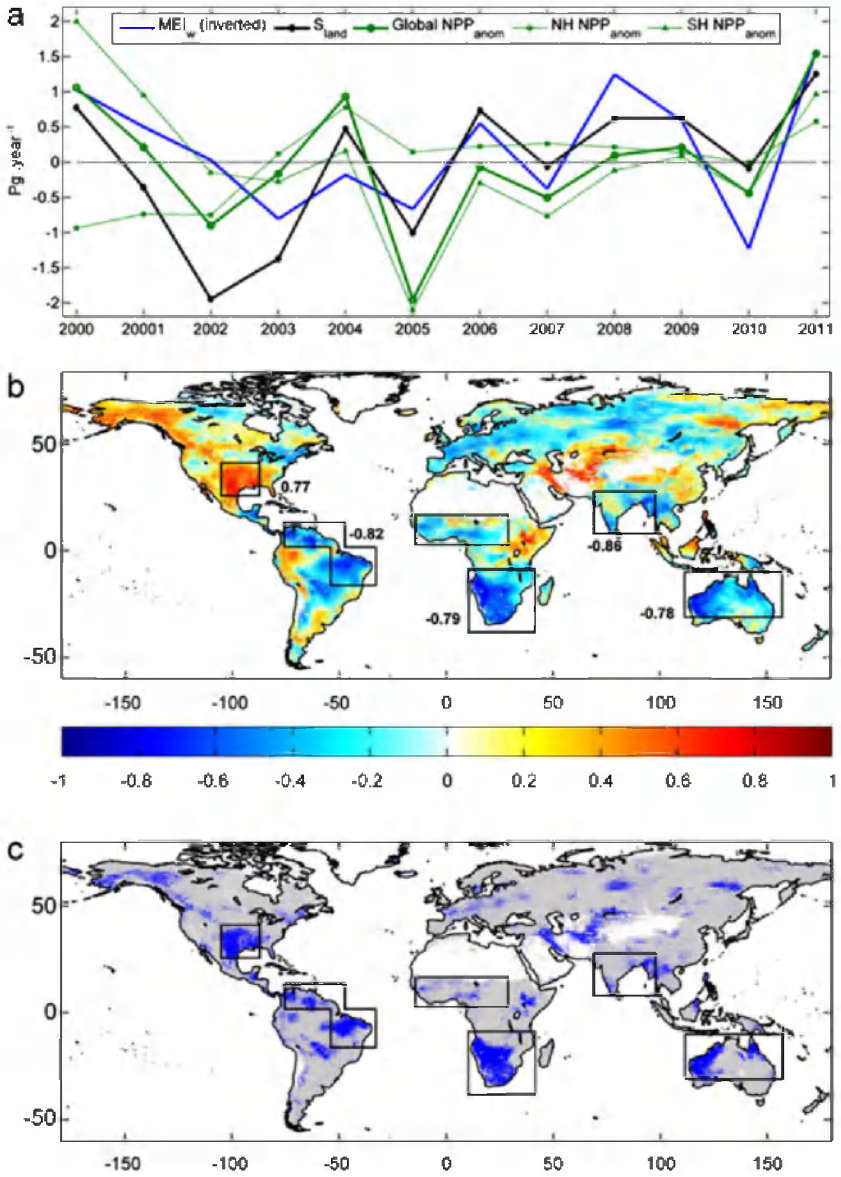

Figure 3. Global, hemispheric, and regional link between ENSO and NPP. (a) Global (green solid), Northern Hemisphere (green dotted), and Southern Hemisphere (green dashed) NPP anom from 2000 to 2011 computed from the MODIS NPP record and detrended Sland for the same period (black solid). The reference NPP mean value is 53.6 Pg year^{-1}. Inverted winter MEI composite (–MEI$_w$, blue solid) computed over the same period. (b) Simple correlation between NPP$_{anom}$ and ENSO computed over the period 2000–2011 for each pixel. (c) Pixels with correlation significant at the 90% level in Figure 3b (blue) and nonsignificant pixels (grey). Rectangular boxes indicate the regions with strong and significant correlations between the variables. Numbers on the side of each box in Figure 3b indicate the overall correlation between the variables over each region.

consequence of the consecutive drought years [*Marengo*, 2004; *Zhao and Running*, 2010] that imply low NPP average values observed for the previous decade.

[28] NPP$_{anom}$ and S$_{land}$ interannual variability were compared for the period 2000–2011 (Figure 3a). A significantly high correlation ($\rho = 0.72, p \ll 0.01$) was found between the two time series, despite the short period, indicating that the interannual variability of both S$_{land}$ and NPP$_{anom}$ is driven (at least partially) by the same patterns.

[29] The analysis of global NPP$_{anom}$ and the partition in NH and SH anomalies (Figure 3a) allows the assessment of the relative contribution of each hemisphere to the high 2011 anomaly as well as to the global interannual variability. Although both hemispheres presented positive anomalies in 2011, the role played by each hemisphere on the global NPP dynamics, it appears to be mainly driven by the SH component which explains 72% ($\rho = -0.85, p \ll 0.01$) of the global NPP$_{anom}$ variance.

[30] The simultaneous analysis of global annual NPP series and MEI$_w$ (with MEI$_w$ signal inverted to facilitate the comparison in the following figures) over 2000–2011 (Figure 3a) indicates very similar variability patterns, with

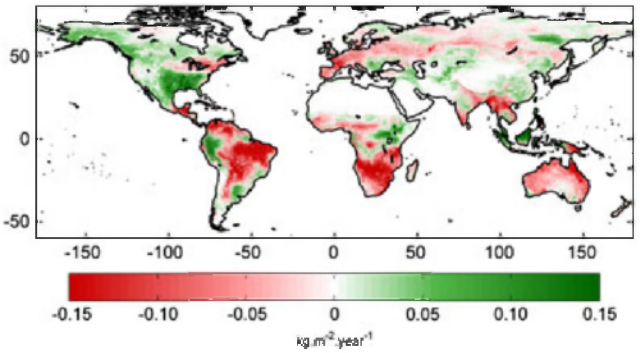

Figure 4. Difference between ENSO$^+$ and ENSO$^-$ in NPP_{anom} composites. The events encompassed on the 2000–2011 record are 2002/2003, 2004/2005, and 2009/2010 (ENSO$^+$) and 1999/2000, 2007/2008, and 2010/2011 (ENSO$^-$).

low global NPP associated to high MEI_w values and high NPP in low MEI_w years, consistently with the results from other works [*Behrenfeld et al.*, 2001; *Nemani et al.*, 2003]. Splitting the results in hemispheric NPP suggests that the covariability between global NPP and ENSO is mainly driven by the SH. The simple correlation between the three time series and MEI_w confirms high anticorrelation values between ENSO and NPP at the global level (ρ = –0.65, p = 0.02) which is very similar for SH (ρ = –0.64, p = 0.03), while for NH the results were not significant. ENSO explains, therefore, a considerable fraction of the global (42%) and SH (41%) NPP variability.

[31] As mentioned above, the use of the longer S_{land} time series allows a more robust assessment of the relationship between global land carbon uptake and ENSO. Moreover, since this data set is completely independent from MODIS data, it reinforces the consistency of the results obtained for the shorter time series of global NPP. Although the results for NPP_{anom} are expected to be somewhat different than the ones found for S_{land}, the similarity of the results obtained for the period 2000–2011 suggests a consistent relationship between ENSO and biospheric carbon uptake, pointing to the existence of both meteorological and biophysical mechanisms driving the response of terrestrial ecosystems to ENSO.

[32] Spatial analysis of correlations allows identifying those regions with strongest response to the ENSO signal and may help to shed some light in the driving physical mechanisms. Thus, the global pattern of correlation coefficient values between ENSO and NPP_{anom} were analyzed on a pixel by pixel basis (Figure 3b). Strong correlations are found worldwide, with negative correlations dominating on the SH, while the NH presents areas characterized by negative (e.g. Europe and Russia) and positive (e.g., North America) sectors that when aggregated, explain the non-significant correlation value obtained for the whole NH. Despite the relatively short (12 years) data set available, it should be emphasized the robustness of the spatial pattern obtained, compatible with the drought areas associated with El Niño events [*Vicente-Serrano et al.*, 2011]. Within the six regions with high NPP anomalies in 2011, five present strong correlations with ENSO: in SAM, SAFR, ASIA, and AUST, NPP is strongly anticorrelated to ENSO while in USA, NPP is positively correlated to ENSO. In SAV, NPP does not have a strong nor significant correlation with ENSO. The average correlation coefficients computed for each of the five regions (values placed next to boxes in Figure 3b) are markedly high, with absolute values above 0.77 ($p \ll 0.01$), meaning that ENSO explains more than half of NPP variability on those areas. The results for SAM and ASIA are particularly high, since ENSO explains more than 67% of the total variance.

[33] Due to the short length of the time series, the relationships described above and the magnitude of ENSO impacts are better analyzed using composites of warm (ENSO$^+$) and cold (ENSO$^-$) phases. The difference in composites of NPP_{anom} obtained during ENSO$^+$ and ENSO$^-$ phases are shown in Figure 4 that provides information about the magnitude of the impact of ENSO on regional NPP. A negative (positive) difference indicates that NPP is decreased (increased) during El Niño and increased (decreased) during La Niña events.

[34] The regions with strong correlation between ENSO and NPP present remarkable differences (either positive or negative) between the two phases, with absolute values in all regions above 0.15 kg m^{-2} $year^{-1}$, with the exception of AUST and most of ASIA. However, the latter regions are mostly composed by arid (AUST) or tropical savannah (ASIA) ecosystems and the differences observed (between 0.05 and 0.1 kg m^{-2} $year^{-1}$) correspond, nevertheless, to a significant fraction of the average low annual productivity from 60% to more than 100% of the average.

[35] These results confirm the relationship found between the total NPP and ENSO on these regions and indicate that in La Niña (El Niño) years, NPP is enhanced (reduced) in the tropical and subtropical sectors of SAM, SAFR, ASIA, and AUST. On the contrary, in USA, El Niño (La Niña) events correspond to high (low) ecosystems' productivity. In the case of 2011, the outstanding La Niña event which lasted for more than 1 year appears, therefore, to have driven the dynamics of ecosystems on the highlighted regions, promoting the very high NPP anomalies observed in SAM, SAFR, ASIA, and AUST and the substantial decline in NPP over USA (Figure 2).

[36] The differences between R_{avg}, T_{avg}, and P_{total} ENSO composites were equally evaluated (Figure 5) and positive (negative) differences are indicative of above (below) average values of each variable during El Niño (La Niña) events. All the regions characterized by significant negative correlation values with ENSO present positive T_{avg} differences between 0.5°C and 2°C, which are especially high in SAFR and AUST (Figure 5a). The opposite occurs in USA, with T_{avg} differences in the range between –1°C and –0.5°C. In the case of both R_{avg} and P_{total}, the signal is not as clear as for T_{avg}. However, negative differences of P_{total} appear to dominate the regions anticorrelated to ENSO, i.e., leading to increased (reduced) precipitation during La Niña (El Niño) events (Figure 5b). In the case of USA, P_{total} presents either positive or negative values, which do not allow for a conclusion to be drawn. For R_{avg}, although the regions with negative correlations with ENSO appear to present a positive difference between phases (i.e., less radiation during La Niña phases), and the opposite behavior for USA, the patterns are also not as strong and consistent as for temperature (Figure 5c).

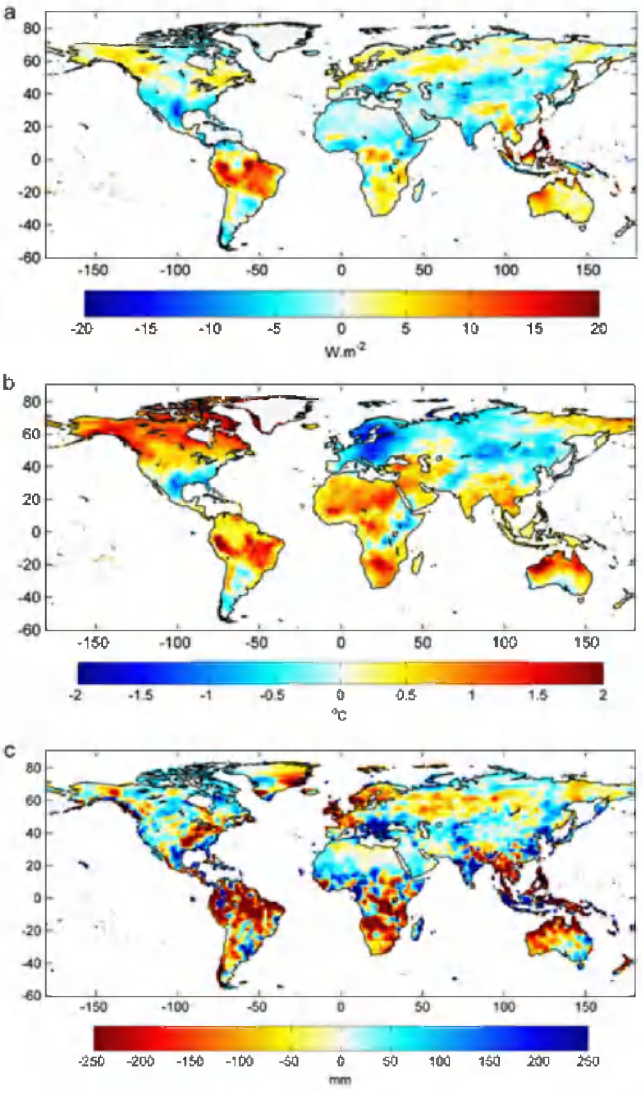

Figure 5. Differences in radiation, temperature, and precipitation between $ENSO^+$ and $ENSO^-$ composites between 2000 and 2011, as in Figure 4, for (a) R_{avg}, (b) T_{avg}, and (c) P_{total}.

[37] The differentiated responses were organized in a global map with the combined response (positive or negative) of T_{avg} and P_{total} to ENSO phases (Figure 6a) and indicated the existence of a similar pattern driving the response of NPP to ENSO variability. The regions anticorrelated to ENSO being dominated by positive T_{avg} and negative P_{total} differences (orange), while USA corresponds to negative differences in T_{avg}, with either positive or negative P_{total} differences. Generally, cooler and wetter conditions are observed during La Niña events in all tropical and subtropical regions negatively correlated to ENSO while warmer and relatively drier conditions are found in USA, although temperature appears to dominate the response in this region. The same analysis was performed including R_{avg}; however, the differentiated response of the variables to ENSO phases appears to be better explained by temperature and precipitation alone and, thus, is not included here.

[38] Cooler conditions may affect directly NPP by reducing autotrophic respiration rates while more rainfall means higher water availability for plant growth. Cooler temperatures also reduce evaporation rates, therefore, increasing soil moisture. Water availability appears, thus, to be the most relevant factor driving the response of NPP to ENSO in the selected regions. This feature is reinforced when analyzing the differences in soil wetness in the top layer (GW_{top}) during positive and negative ENSO phases (Figure 6b). Negative differences, i.e., wetter (drier) conditions during La Niña (El Niño) phases, dominate all the regions anticorrelated with ENSO while positive differences, i.e., drier (wetter) conditions during La Niña (El Niño) are observed in USA. The same patterns, although attenuated, are found in GW_{root} (Figure 6c), confirming a strong enhancement (suppression) in soil water availability for plant functioning and growth during La Niña (El Niño) phases in those

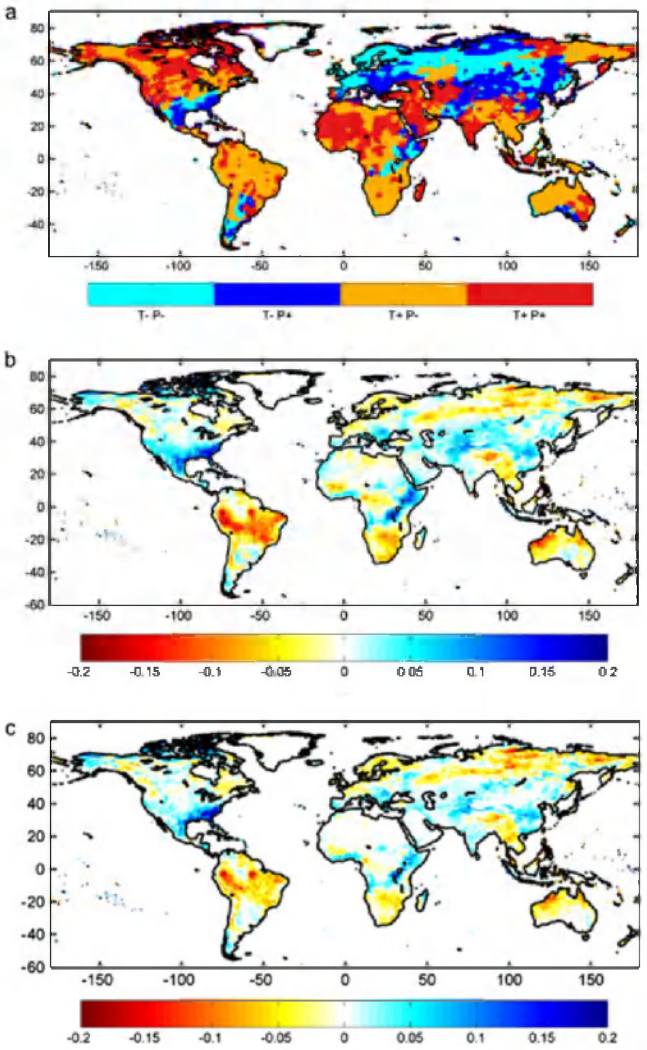

Figure 6. Summary of temperature and precipitation influence on water availability between positive and negative ENSO phases. (a) Combinations of the signals of T_{avg} and P_{total} differences between $ENSO^+$ and $ENSO^-$ composites. For example, T– P– corresponds to negative differences in both T_{avg} and P_{total}, T– P+ to negative differences in T_{avg} and positive in P_{total}. Difference between $ENSO^+$ and $ENSO^-$ composites for (b) GW_{top} and (c) GW_{root}.

regions where negative (positive) correlations between NPP and ENSO are found.

[39] It should be stressed that we have repeated this analysis using a longer period (1979–2012 for T_{avg}, R_{avg}, GW_{top}, and GW_{root} and 1986–2012 for P_{total}) and the patterns obtained (not shown) are in good agreement with those presented here, namely for the selected regions, being also in accordance with previous studies focused on the impact of ENSO on those variables [*Mason and Goddard*, 2001; *Marengo*, 2004; *McPhaden et al.*, 2006]. Furthermore, results were also compared to NCEP/DOE II Reanalyzes (not shown) and the obtained patterns revealed to be consistent with the ones presented in Figures 5 and 6. We must acknowledge that in some tropical areas (e.g., Amazon), the main limiting factor, besides water availability, is solar radiation and not temperature per se [*Samanta et al.*, 2010], but the core sector of the Amazon forest does not exhibit a significant correlation to ENSO and therefore was not included in our regional analysis.

4. Conclusions

[40] The year of 2011 can be regarded as a remarkable year: presenting the highest land sink value since 1959 [*Le Quéré et al.*, 2012] and, as shown here, holding also the highest value of global NPP on the MODIS record (2000–2011). In this study we provide evidence that the coupled pattern of El Niño/Southern Oscillation controls much of the temporal and spatial variability observed in vegetation carbon uptake, thus affecting indirectly the airborne fraction.

[41] The results provide insights on the nature and the strength of the relationship between ENSO and global NPP. The fact that ENSO accounts for more than 40% of interannual variability of carbon uptake by global ecosystems (2000–2011) provides a new perspective to the assessment of long-term NPP variability, either when evaluating past trends but also when trying to put it in context in future projections. We are confident that our results are relatively robust, although we must acknowledge the caveats of using relatively short time NPP series. Nevertheless, this caveat is hampered by the simultaneous analysis performed with the much longer land sink data set that reinforces the links with the ENSO signal corroborating the role played by the 2011 year La Niña in the record NPP and land sink values.

[42] This work proposes a simple physical mechanism driving the response of NPP to ENSO variability, through changes in soil water balance and stresses the importance water availability in the dynamics of vegetation productivity. The fact that the same mechanism appears to be driving the ecosystems' response to ENSO is a striking result given the different geographical settings of each region, in different continents, at different latitudes and comprising different biomes, which have been described to have different limiting factors [*Nemani et al.*, 2003]. Previous works suggested that drought in Amazonia could be one of the major drivers of global productivity [*Cox et al.*, 2004; *Zhao and Running*, 2010]; here we show that the cumulative effect of other regions, most located in the subtropical regions in the Southern Hemisphere, appears to have a strong influence on the variability of global NPP, driven by water deficits/surpluses related to ENSO dynamics.

[43] **Acknowledgments.** Ana Bastos was funded by Portuguese for Science and Technology (SFRH/BD/78068/2011), by Calouste Gulbenkian Foundation, and by Fulbright Commission Portugal (grant ID 15122932). Steven W. Running was sponsored by the MODIS Project (grant NNX11AF18G). This work was partially supported by Project QSECA (PTDC/AAG-GLO/4155/2012) funded by the Portuguese Foundation for Science and Technology (FCT). The authors acknowledge the comments from Sergio Vicente-Serrano.

References

Ahlström, A., P. A. Miller, and B. Smith (2012), Too early to infer a global NPP decline since 2000, *Geophys. Res. Lett.*, *39*, L15403, doi:10.1029/2012GL052336.

Ballantyne, A. P., C. B. Alden, J. B. Miller, P. P. Tans, and J. W. C. White (2012), Increase in observed net carbon dioxide uptake by land and oceans during the past 50 years, *Nature*, *488*(7409), 70–72.

Beer, C., et al. (2010), Terrestrial gross carbon dioxide uptake: Global distribution and covariation with climate, *Science*, *329*(5993), 834–838, doi:10.1126/science.1184984.

Behrenfeld, M. J., et al. (2001), Biospheric primary production during an ENSO transition, *Science*, *291*(5513), 2594–2597, doi:10.1126/science.1055071.

Blunden, J., and D. S. Arndt (2012), State of the climate in 2011, *Bull. Am. Meteorol. Soc.*, *93*(7), S1–S282, doi:10.1175/2012BAMSStateoftheClimate.1.

Boening, C., J. K. Willis, F. W. Landerer, R. S. Nerem, and J. Fasullo (2012), The 2011 La Niña: So strong, the oceans fell, *Geophys. Res. Lett.*, *39*, L19602, doi:10.1029/2012GL053055.

Chapin, I., et al. (2006), Reconciling carbon-cycle concepts, terminology, and methods, *Ecosystems*, *9*(7), 1041–1050.

Ciais, P., et al. (2005), Europe-wide reduction in primary productivity caused by the heat and drought in 2003, *Nature*, *437*(7058), 529–533.

Cox, P. M., R. A. Betts, M. Collins, P. P. Harris, C. Huntingford, and C. D. Jones (2004), Amazonian forest dieback under climate-carbon cycle projections for the 21st century, *Theor. Appl. Climatol.*, *78*(1-3), 137–156, doi:10.1007/s00704-004-0049-4.

Diaz, H. F., M. P. Hoerling, and J. K. Eischeid (2001), ENSO variability, teleconnections and climate change, *Int. J. Climatol.*, *21*(15), 1845–1862, doi:10.1002/joc.631.

Evans, J. P., and I. Boyer-Souchet (2012), Local sea surface temperatures add to extreme precipitation in northeast Australia during La Niña, *Geophys. Res. Lett.*, *39*, L10803, doi:10.1029/2012GL052014.

Friedlingstein, P., and I. Prentice (2010), Carbon-climate feedbacks: A review of model and observation based estimates, *Curr. Opin. Environ. Sustainability*, *2*(4), 251–257, doi:10.1016/j.cosust.2010.06.002.

Heimann, M., and M. Reichstein (2008), Terrestrial ecosystem carbon dynamics and climate feedbacks, *Nature*, *451*(7176), 289–292.

Huete, A. R., K. Didan, Y. E. Shimabukuro, P. Ratana, S. R. Saleska, L. R. Hutyra, W. Yang, R. R. Nemani, and R. Myneni (2006), Amazon rainforests green-up with sunlight in dry season, *Geophys. Res. Lett.*, *33*, L06405, doi:10.1029/2005GL025583.

Jones, C. D., and P. M. Cox (2001), Modeling the volcanic signal in the atmospheric CO_2 record, *Global Biogeochem. Cycles*, *15*(2), 453–465, doi:10.1029/2000GB001281.

Kanamitsu, M., W. Ebisuzaki, J. Woollen, S.-K. Yang, J. J. Hnilo, M. Fiorino, and G. L. Potter (2002), NCEP/DOE AMIP-II Reanalysis (R-2), *Bull. Am. Meteorol. Soc.*, *83*(11), 1631–1643, doi:10.1175/BAMS-83-11-1631.

Le Quéré, C., et al. (2009), Trends in the sources and sinks of carbon dioxide, *Nat. Geosci.*, *2*(12), 831–836.

Le Quéré, C., et al. (2012), The global carbon budget 1959–2011, *Earth Syst. Sci. Data Discuss.*, *5*(2), 1107–1157, doi:10.5194/essdd-5-1107-2012.

Marengo, J. A. (2004), Interdecadal variability and trends of rainfall across the Amazon basin, *Theor. Appl. Climatol.*, *78*, 79–96, doi:10.1007/s00704-004-0045-8.

Mason, S. J., and L. Goddard (2001), Probabilistic precipitation anomalies associated with ENSO, *Bull. Am. Meteorol. Soc.*, *82*(4), 619–638.

McPhaden, M. J., S. E. Zebiak, and M. H. Glantz (2006), ENSO as an integrating concept in earth science, *Science*, *314*(5806), 1740–1745, doi:10.1126/science.1132588.

Nemani, R. R., C. D. Keeling, H. Hashimoto, W. M. Jolly, S. C. Piper, C. J. Tucker, R. B. Myneni, and S. W. Running (2003), Climate-

driven increases in global terrestrial net primary production from 1982 to 1999, *Science*, *300*(5625), 1560–1563, doi:10.1126/science.1082750.

Piao, S., et al. (2008), Net carbon dioxide losses of northern ecosystems in response to autumn warming, *Nature*, *451*(7174), 49–52.

Raupach, M. R. (2011), Carbon cycle: Pinning down the land carbon sink, *Nat. Clim. Change*, *1*(3), 148–149.

Rienecker, M. M., et al. (2011), MERRA: NASA's Modern-Era Retrospective Analysis for Research and Applications, *J. Clim.*, *24*(14), 3624–3648, doi:10.1175/JCLI-D-11-00015.1.

Rudolf, B., and U. Schneider (2005), Calculation of gridded precipitation data for the global land-surface using in-situ gauge observations, in *Proceedings of the 2nd Workshop of the International Precipitation Working Group IPWG,Monterey October 2004*, pp. 231-247. EUMETSAT, iSBN 92-9110-070-6, ISSN 1727-432X.

Running, S. W., R. R. Nemani, F. A. Heinsch, M. Zhao, M. Reeves, and Hashimoto H. (2004), A continuous satellite-derived measure of global terrestrial primary production, *BioScience*, *54*(6), 547–560.

Vicente-Serrano, S. M., J. I. López-Moreno, L. Gimeno, R. Nieto, E. Morán-Tejeda, J. Lorenzo-Lacruz, S. Beguería, and C. Azorin-Molina (2011), A multiscalar global evaluation of the impact of ENSO on droughts, *J. Geophys. Res.*, *116*, D20109, doi:10.1029/2011JD016039.

Samanta, A., S. Ganguly, H. Hashimoto, S. Devadiga, E. Vermote, Y. Knyazikhin, R. R. Nemani, and R. B. Myneni (2010), Amazon forests did not green-up during the 2005 drought, *Geophys. Res. Lett.*, *37*, L05401, doi:10.1029/2009GL042154.

Samanta, A., M. H. Costa, E. L. Nunes, S. A. Vieira, L. Xu, and R. B. Myneni (2011), Comment on "Drought-induced reduction in global terrestrial net primary production from 2000 through 2009", *Science*, *333*(6046), 1093, doi:10.1126/science.1199048.

Sarmiento, J. L., M. Gloor, N. Gruber, C. Beaulieu, A. R. Jacobson, S. E. Mikaloff Fletcher, S. Pacala, and K. Rodgers (2010), Trends and regional distributions of land and ocean carbon sinks, *Biogeosciences*, *7*(8), 2351–2367, doi:10.5194/bg-7-2351-2010.

Zhao, M., and S. W. Running (2010), Drought-induced reduction in global terrestrial net primary production from 2000 through 2009, *Science*, *329*(5994), 940–943, doi:10.1126/science.1192666.